ARTICLES

Journal of Semiconductors
(2022) 43, 112501
doi: 10.1088/1674-4926/43/11/112501

$(Ba_{1-x}Na_x)F(Zn_{1-x}Mn_x)Sb$: A novel fluoride-antimonide magnetic semiconductor with decoupled charge and spin doping

Xueqin Zhao[1], Jinou Dong[1], Licheng Fu[1], Yilun Gu[1], Rufei Zhang[1], Qiaolin Yang[1], Lingfeng Xie[1], Yinsong Tang[1], and Fanlong Ning[1, 2, 3, †]

[1]Zhejiang Province Key Laboratory of Quantum Technology and Device and Department of Physics, Zhejiang University, Hangzhou 310027, China

[2]Collaborative Innovation Center of Advanced Microstructures, Nanjing University, Nanjing 210093, China

[3]State Key Laboratory of Silicon Materials, Zhejiang University, Hangzhou 310027, China

Abstract: We report the successful synthesis and characterization of a novel 1111-type magnetic semiconductor $(Ba_{1-x}Na_x)$-$F(Zn_{1-x}Mn_x)Sb$ ($0.05 \leqslant x \leqslant 0.175$) with tetragonal ZrSiCuAs-type structure, which is isostructural to the layered iron-based superconductor La(O,F)FeAs. Na substitutions for Ba and Mn substitutions for Zn introduce carriers and local magnetic moments, respectively. Ferromagnetic interaction is formed when Na and Mn are codoped, demonstrating that local magnetic moments are mediated by carriers. Iso-thermal magnetization shows that the coercive field is as large as ~ 12 000 Oe, which is also reflected in the large split between the temperature-dependent magnetization in zero-field-cooling and field-cooling condition. AC susceptibility under zero field demonstrates that samples evolve into spin-glass state below spin freezing temperature T_f. The measurements of temperature-dependent resistivity indicate that $(Ba_{1-x}Na_x)F(Zn_{1-x}Mn_x)Sb$ exhibits semiconducting behaviour.

Key words: magnetic semiconductors; ferromagnetic interaction; carriers; spin-glass

Citation: X Q Zhao, J O Dong, L C Fu, Y L Gu, R F Zhang, Q L Yang, L F Xie, Y S Tang, and F L Ning, $(Ba_{1-x}Na_x)F(Zn_{1-x}Mn_x)Sb$: A novel fluoride-antimonide magnetic semiconductor with decoupled charge and spin doping[J]. *J. Semicond.*, 2022, 43(11), 112501. https://doi.org/10.1088/1674-4926/43/11/112501

1. Introduction

Due to the potential applications in spintronics devices, diluted magnetic semiconductors (DMSs) that simultaneously combine the spin and charge degrees of electrons have received extensive attentions[1–6]. In 1990s, the III–V DMS (Ga,Mn)As was successfully prepared by low temperature molecular beam epitaxy (LT-MBE) method. The Curie temperature T_C has reached as high as ~200 K[7–9], which is much higher than those of some II–VI DMSs, such as (Zn,Mn)Te[10] and (Cd,Mn)Te[11]. To explain the magnetic mechanism of III–V DMSs, Dietl *et al.* proposed a mean-field Zener's model that described the ferromagnetic interactions between the local magnetic moments and carriers, and predicted that T_C of some DMSs may reach room temperature if more Mn atoms are doped[12, 13]. Subsequently, Reed *et al.* reported that T_C of (Ga,Mn)N was up to ~370 K[14]. The application of DMSs in spintronic devices will be practical once the Curie temperature of some DMSs are above room temperature. However, the development of III–V DMSs has also encountered some limitations. For example, in (Ga,Mn)As, magnetic atoms Mn easily enter the interstitial positions of the lattice, which makes it difficult to accurately determine the actual amount of doped Mn atoms. Meanwhile, the substitutions of Mn for Ga introduce magnetic moments and carriers simultaneously, which constrains us to study their individual contribution to the formation of the ferromagnetic ordering. In addition, films cannot be used for microscopic probes that are based on bulk materials, such as nuclear magnetic resonance (NMR), neutron scattering and muon spin relaxation (μSR)[5, 15–17]. On that account, the study of bulk DMSs with decoupled charge and spin doping are worthy of attentions.

Recently, many bulk Zn-based DMSs derived from Fe-based superconductors have been reported. Foremost, according to the pioneer theory work of Masek *et al.*[18], Deng *et al.*[16] prepared a new 111-type DMS Li(Zn,Mn)As, which is isostructural to Fe-based superconductor LiFeAs[19]. This is the first bulk DMS that carriers and magnetic moments could be controlled independently. In I–II–V semiconductor LiZnAs, doping excessive Li introduces carriers and Mn substitutions for Zn introduce local moments, and the Curie temperature T_C is ~50 K. Until now, the highest Curie temperature recorded is a 122-type DMS $(Ba,K)(Zn,Mn)_2As_2$ with T_C up to ~230 K[20, 21], which has surpassed that of (Ga,Mn)As. In addition, Ding *et al.*[17] synthesized a 1111-type DMS (La,Ba)(Zn,Mn)AsO with T_C up to ~40 K. μSR measurements have proved that the ferromagnetic ordering of these DMSs is intrinsic rather than caused by magnetic clusters or impurities. Moreover, μSR measurements reveal that Li(Zn,Mn)As, $(Ba,K)(Zn,Mn)_2As_2$ and (La,Ba)(Zn,Mn)AsO share the same mechanism of magnetic origin as that of (Ga,Mn)As[16, 17, 20, 22]. That is to say, searching for more new DMSs materials will help us to understand the general mechanism of magnetic ordering in all DMSs, and direct us to optimize the choices of materials.

In this paper, we report the successful fabrication of a

Correspondence to: F L Ning, ningfl@zju.edu.cn
Received 2 JUNE 2022; Revised 16 JULY 2022.

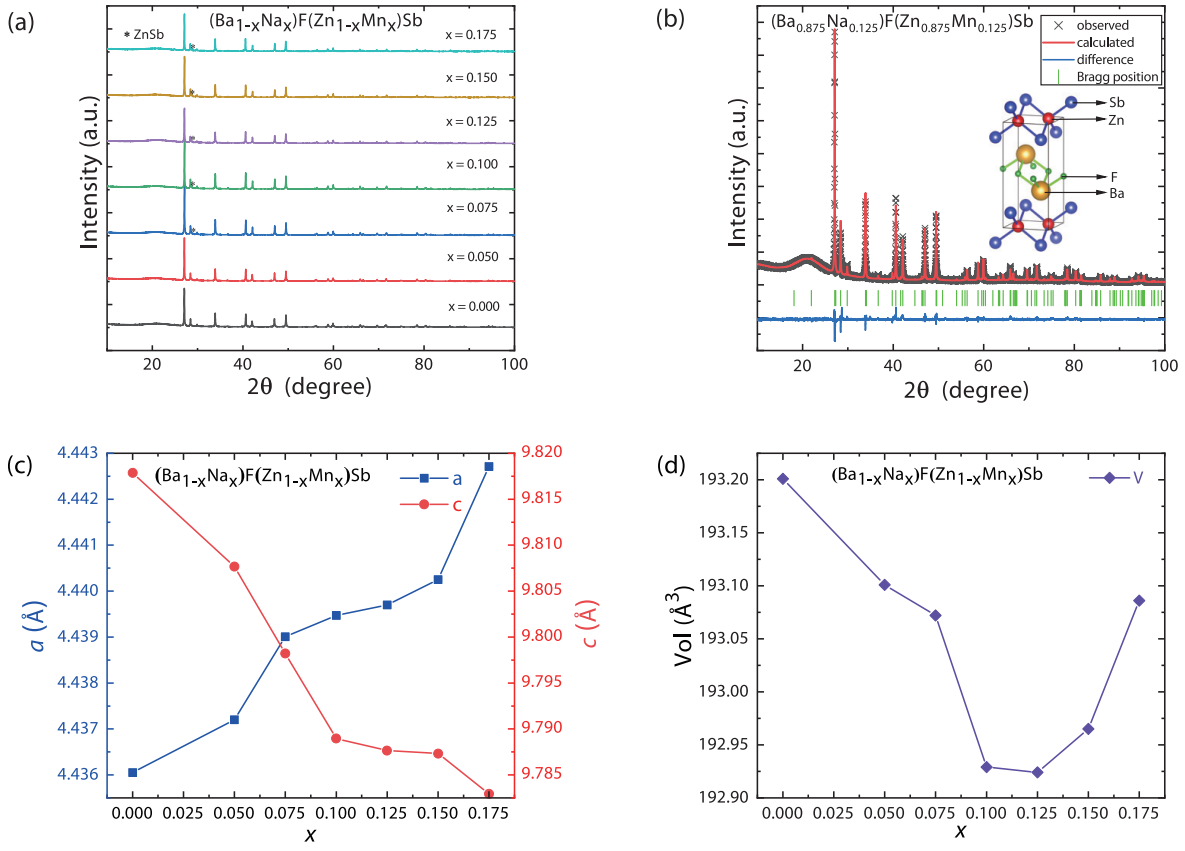

Fig. 1. (Color online) (a) The polycrystal powder X-ray diffraction patterns of $(Ba_{1-x}Na_x)F(Zn_{1-x}Mn_x)Sb$ (x = 0.00, 0.05, 0.075, 0.10, 0.125, 0.15, and 0.175). Traces of impurities ZnSb are marked as stars (*). (b) The Rietveld refinement result of $(Ba_{0.875}Na_{0.125})F(Zn_{0.875}Mn_{0.125})Sb$. Inset shows the tetragonal ZrCuSiAs-type crystal structure of parent compound BaFZnSb. (c) Lattice parameters a and c versus doping level x of $(Ba_{1-x}Na_x)F(Zn_{1-x}Mn_x)Sb$ (x = 0.00, 0.05, 0.075, 0.10, 0.125, 0.15, and 0.175). (d) The unit cell volume of $(Ba_{1-x}Na_x)F(Zn_{1-x}Mn_x)Sb$ (x = 0.00, 0.05, 0.075, 0.10, 0.125, 0.15, and 0.175).

new 1111-type magnetic semiconductor, $(Ba_{1-x}Na_x)F(Zn_{1-x}Mn_x)Sb$ (x = 0.05, 0.075, 0.1, 0.125, 0.15, and 0.175), via doping Na into Ba sites and Mn into Zn sites in the parent compound BaFZnSb to introduce hole carriers and local magnetic moments, respectively. BaFZnSb shares the same crystal structure with that of LaOZnAs and LaOCuS, which have been reported to be the parent semiconductors of 1111-type DMSs (La,Ba)O(Zn,Mn)As (T_C ~ 40 K)[17] and (La,Sr)O(Cu,Mn)S (T_C ~ 200 K)[23], respectively. Comparing with oxides, the ionic radius of fluoride is smaller and its electronegativity is stronger, which results in constituting stronger ionic bonds[24]. The Weiss temperature θ of $(Ba_{1-x}Na_x)F(Zn_{1-x}Mn_x)Sb$ is up to ~ 16 K for x = 0.175, which is a sign of ferromagnetic interaction, and followed by a magnetic glassy transition below T_f ~ 14 K.

2. Experiments

We synthesized the polycrystalline specimens of $(Ba_{1-x}Na_x)F(Zn_{1-x}Mn_x)Sb$ through the solid-state reaction method. High-purity starting materials Ba (99.2%, Alfa Aesar), BaF_2 (99.99%, Aladdin), Na (99.7%, Aladdin), Zn (99.9%, Alfa Aesar), Mn (99.95%, Alfa Aesar) and Sb (99.999%, Prmat) were mixed according to stoichiometric proportions and were placed in alumina crucibles before sealing in evacuated silica tubes. The mixture was heated slowly to 200 °C and held for 10 h, then heated to 750 °C and held for another 10 h, followed by furnace cooling to room temperature. After that, the intermediate products were grounded, pressed into pellets, placed in alumina crucibles, sealed in evacuated silica tubes again and then reheated to 750 °C for 30 h. To protect the contamination from air and H_2O, all operations except the sealing of silica tubes were executed in a glove box filled with high-purity Ar (O_2 and H_2O < 0.1 ppm).

The crystal structures of the samples were characterized at room temperature by a powder X-ray diffractometer (Model EMPYREAN) using monochromatic Cu-$K_{\alpha 1}$ radiation with $\lambda(K_{\alpha 1})$ = 1.540598 Å. The detailed information of lattice constants and unit cell volume was calculated by Rietveld refinement method using the GSAS-II software package[25]. The DC magnetization measurements were performed on a quantum design magnetic property measurement system (MPMS). The AC susceptibility measurements were measured on a quantum design physical property measurement system (PPMS). The electrical resistivity measurements were conducted on sintered pellets by the four-probe method.

3. Results and discussion

In Fig. 1(a), we show the powder X-ray diffraction patterns of polycrystals $(Ba_{1-x}Na_x)F(Zn_{1-x}Mn_x)Sb$ with x = 0.00, 0.05, 0.075, 0.1, 0.125, 0.15, and 0.175, respectively. The Bragg peaks can be well indexed by a ZrSiCuAs-type tetragonal structure with space group P4/nmm[26], which is isostructural to the 1111-type superconductor La(F,O)FeAs[27], indicating that Na substitution for Ba and Mn substitution for Zn have no influence on the tetragonal crystal structure. In Fig. 1(b), we show the Rietveld refinement result of $(Ba_{0.875}Na_{0.125})F$-

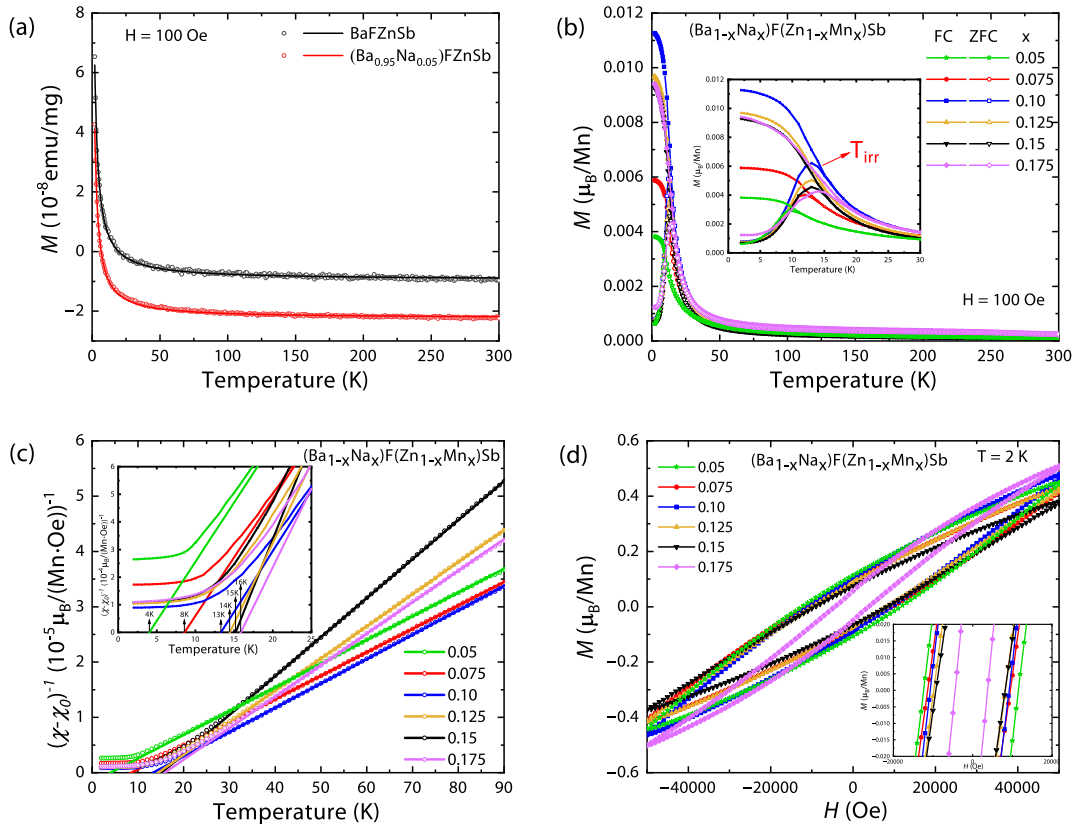

Fig. 2. (Color online) (a) The temperature dependence of DC magnetization for parent phase BaFZnSb and $(Ba_{0.95}Na_{0.05})FZnSb$ under field-cooling mode in an external magnetic field of 100 Oe. The data (open circles) are the data dots, and the solid lines are the Curie-Weiss fitting results. (b) The temperature dependent magnetization (M) for $(Ba_{1-x}Na_x)F(Zn_{1-x}Mn_x)Sb$ (x = 0.05, 0.075, 0.10, 0.125, 0.15 and 0.175) in both zero-field-cooling (ZFC) and field-cooling (FC) procedures under an external magnetic field of 100 Oe. Inset shows the enlarged M(T) curves for all specimens at low temperature. Arrow marks T_{irr} for x = 0.10. (c) The plot of $1/(\chi - \chi_0)$ versus T for $(Ba_{1-x}Na_x)F(Zn_{1-x}Mn_x)Sb$ (x = 0.05, 0.075, 0.10, 0.125, 0.15 and 0.175) under FC condition. Arrows mark the Weiss temperatures. Inset shows the enlarged plot of $1/(\chi - \chi_0)$ versus T for all of specimens below 30 K. (d) Iso-thermal magnetization for $(Ba_{1-x}Na_x)F(Zn_{1-x}Mn_x)Sb$ (x = 0.05, 0.075, 0.10, 0.125, 0.15 and 0.175) at 2 K. Inset shows the enlarged $M(H)$ curves for all of specimens under an external magnetic field B_{ext} from −20 000 to 20 000 Oe.

$(Zn_{0.875}Mn_{0.125})Sb$. The resultant weighted reliable factor R_{wp} is 7.962%, indicating the samples are in good quality. With doping level x increasing, some small peaks of ZnSb impurities marked as * in Fig. 1(a) were observed. ZnSb impurities are non-magnetic, thus they will not affect the discussion of magnetism in the following.

As shown in Fig. 1(b), the parent compound BaFZnSb has a layered crystal structure, which consists of two layers in the ab plane: one is $[BaF]^+$ layers (BaF_4 tetrahedra) and the other is $[ZnSb]^-$ layers ($ZnSb_4$ tetrahedra)[28]. These layers are conventionally regarded as the tetragonal fluorite and anti-fluorite structure types separately[28], and they are stacked alternately along the c-axis. The lattice parameters obtained from Rietveld refinement are shown in Fig. 1(c). The lattice parameters of parent compound BaFZnSb are a = 4.43605 Å and c = 9.81786 Å, which is close to previous reported values of a = 4.4384 Å and c = 9.7789 Å[28]. Meanwhile, with doping level x increasing, a monotonically increases from 4.43720 to 4.44271 Å, and c continuously decreases from 9.80767 to 9.78259 Å, repectively. This should be ascribed to the fact that the ionic radius of Na^+ (1.02 Å) is smaller than that of Ba^{2+} (1.35 Å), but the ionic radius of Mn^{2+} (0.83 Å) is larger than that of Zn^{2+} (0.74 Å). The monotonical behaviours of lattice parameters a and c with doping level x demonstrate the successful doping of Na into Ba sites and Mn into the Zn sites, respectively. In Fig. 1(d), we find that the unit cell volume doesn't vary monotonically with increasing doping level x. This is due to the fact that lattice parameters a and c behave in opposite direction.

We show DC magnetization (M) measurements of the parent phase BaFZnSb and $(Ba_{0.95}Na_{0.05})FZnSb$ under field-cooling condition with an external field B_{ext} = 100 Oe in Fig. 2(a). We find that the magnetization for both samples is very small, ~10^{-8} emu/mg, confirming the characteristic of paramagnetism. By using the Curie-Weiss law to fit the data, we get the values of Weiss temperatures as −0.7 and −0.6 K, respectively. This also demonstrates that both BaFZnSb and $(Ba_{0.95}Na_{0.05})FZnSb$ are in paramagnetic ground state. That is to say, doping only carriers can not introduce any type of magnetic phase transition. This is similar to the situation in SrF(Zn,Cu)Sb[29], where doping only Cu into SrFZnSb does not induce any magnetic ordering.

In Fig. 2(b), we show the temperature-dependent magnetization (M) in both zero-field-cooling (ZFC) and field-cooling (FC) procedures under an applied external field B_{ext} = 100 Oe for $(Ba_{1-x}Na_x)F(Zn_{1-x}Mn_x)Sb$ (x = 0.05, 0.075, 0.1, 0.125, 0.15 and 0.175). There is an obvious increase for the magnetic moment at low temperature. Also, ZFC and FC curves abruptly split at a temperature defined as T_{irr} (as marked by the arrow in the inset of Fig. 2(b)) for all doping levels, which is related

Table 1. The Weiss temperature θ, the base temperature magnetic moment M_{base}, the effective magnetic moment μ_{eff} and the coercive field H_C for $(Ba_{1-x}Na_x)F(Zn_{1-x}Mn_x)Sb$ for $x = 0.05$, 0.075, 0.10, 0.125, 0.15 and 0.175.

x	θ (K)	M_{base} (μ_B/Mn)	μ_{eff} (μ_B/Mn)	H_C (Oe)
0.05	4	0.00383	3.23	12000
0.075	8	0.00588	3.25	10500
0.10	13	0.01127	3.18	10000
0.125	14	0.00969	2.77	9000
0.15	15	0.00927	2.52	8700
0.175	16	0.00941	2.80	4000

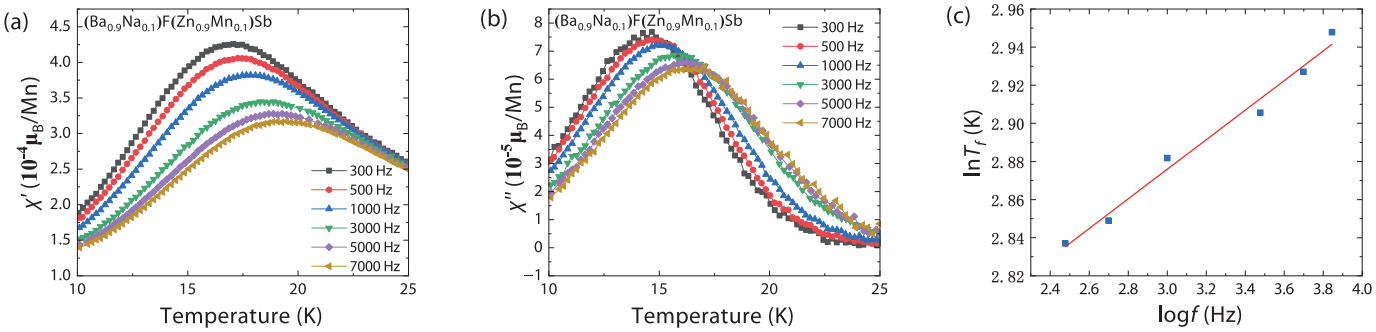

Fig. 3. (Color online) The (a) real part χ' and (b) imaginary part χ'' of AC susceptibility with varying frequencies f under zero field for $(Ba_{0.9}Na_{0.1})F(Zn_{0.9}Mn_{0.1})Sb$. (c) A frequency dependence of spin freezing temperature T_f for $(Ba_{0.9}Na_{0.1})F(Zn_{0.9}Mn_{0.1})Sb$.

to the pinning of the domain wall[30]. In Fig. 2(b), for $(Ba_{0.9}Na_{0.1})F(Zn_{0.9}Mn_{0.1})Sb$, the split between FC and ZFC curves is at $T_{irr} \sim 16$ K, and the maximum of ZFC curve is at $T_f \sim 13$ K. On the other hand, the magnetic moments (M_{base}) at base temperature of 2 K under FC mode increase from 0.0038 μ_B/Mn for $x = 0.05$ to 0.0112 μ_B/Mn for $x = 0.10$, and then decrease to 0.0092 μ_B/Mn for $x = 0.15$. In the inset of Fig. 2(b), we can clearly observe the variation of magnetic moments under low temperature for specimens with $x = 0.05$, 0.075, 0.1, 0.125, 0.15 and 0.175, respectively. The increasing M_{base} for $x \leqslant 0.1$ may be attributed to the formation and enhancement of ferromagnetic interaction. M_{base} decreases for $x \geqslant 0.125$, which might be generated by the competition between local ferromagnetic coupling through the indirect exchange interaction and antiferromagnetic coupling caused by direct exchange interaction existing in Mn atoms at nearest-neighbour (N.N.) Zn sites. This is also a piece of evidence that too many Mn atoms doping is detrimental to the ferromagnetic interaction, as shown in many types of DMSs, such as (La,Sr)(Zn,Mn)SbO[31] and $(Ca,Na)(Zn,Mn)_2Sb_2$[32]. The probability that two Mn atoms are at N.N. sites satisfies $P = C_4^1 x(1-x)^3$. For example, for the doping level of $x = 0.1$, for a Mn atom finding one Mn atom at its N.N. sites is $P = C_4^1 \times 0.1 \times 0.9^3 = 29.16\%$, and P increases to 36.85% for $x = 0.15$. That is, as the Mn doping level x continues to rise, the enhanced antiferromagnetic interaction suppresses the ferromagnetic interation.

When the temperature is much higher than the Curie temperature, the magnetic susceptibility generally satisfies the Curie-Weiss law, $\chi = \chi_0 + C/(T-\theta)$, where χ_0 is a temperature-independent component, C is the Curie constant and θ is Weiss temperature. In Fig. 2(c), we plot $1/(\chi - \chi_0)$ versus temperature. The intersections of the fitting lines and the x-axis are the Weiss temperatures θ. All values of θ are positive, further identifying the establishment of ferromagnetic interaction between Mn atoms. Moreover, Zn/Mn-Sb bond length is longer than that of Zn/Mn-As, and Sb-Zn/Mn-Sb bond angle α is further away from the ideal α value in non-distorted ideal tetrahedron as that of As-Zn/Mn-As[33]. On that account, compared with that of (Ba,K)F(Zn,Mn)As[34], the Weiss temperature of our samples is lower. In addition, we also apply the formula $C = N\mu_0\mu_{eff}^2/3k_B$ to obtain effective magnetic moment μ_{eff}, and put these numbers in Table 1.

In Fig. 2(d), we present the iso-thermal magnetization at 2 K for $(Ba_{1-x}Na_x)F(Zn_{1-x}Mn_x)Sb$ ($x = 0.05$, 0.075, 0.1, 0.125, 0.15 and 0.175). Clear hysteresis loops are observed, which indicates the presence of ferromagnetic interaction. With the increasing of doping level x, the coercive field H_C decreases. In particular, the largest H_C is up to ~12 000 Oe, which is also reflected in the large differences between the measurements of temperature-dependent magnetization (M) in ZFC and FC condition at T_{irr}. The large coercive field H_C is similar to that in (La,Ba)(Zn,Mn)AsO[17] and (Ba,K)F(Zn,Mn)As[34], but much larger than that in Li(Zn,Mn)As[16] and $Cu_2(Zn,Mn)(Sn,Al)Se_4$[35]. Comparing the crystal structures of two kinds of materials mentioned above, we find that the coercive fields seem to be much larger in crystals with layered structure. We list all parameters obtained above in Table 1.

We observe that the magnetization has not even reached saturation at 2 K under the maximum external magnetic field as high as 5 T in Fig. 2(d), which is a characteristic of spin-glass systems. Therefore, we perform AC susceptibility with varying frequencies f under zero field for $(Ba_{0.9}Na_{0.1})F(Zn_{0.9}Mn_{0.1})Sb$. The real part χ' and imaginary part χ'' of the AC susceptibility are shown in Figs. 3(a) and 3(b), respectively. As the frequency increases, the cusp temperature, T_f, shifts to higher temperature on both real part χ' and imaginary part χ'', and the overall magnitude of real part χ' slightly decreases. We apply the equation $K = \Delta T_f/[T_f \Delta \log f]$ to describe the f-dependence of T_f[36]. The value of K obtained in Fig. 3(c) is ~ 0.077, which is within the range between 0.005 to 0.08 of conventional spin-glass systems[37], indicat-

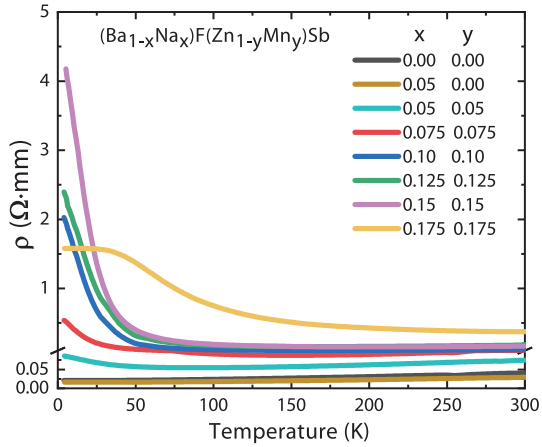

Fig. 4. (Color online) Temperature-dependent resistivity measurements for $(Ba_{1-x}Na_x)F(Zn_{1-y}Mn_y)Sb$ (x = 0.00, y = 0.00; x = 0.05, y = 0.00; x = 0.05, y = 0.05; x = 0.075, y = 0.075; x = 0.10, y = 0.10; x = 0.125, y = 0.125; x = 0.15, y = 0.15; x = 0.175, y = 0.175).

ing our samples evolve into spin-glass state below T_f. Similar behaviour has also been observed in other DMSs, such as $Ba(Zn,Cu,Mn)_2As_2$[38] and $(Ba,K)(Zn,Mn)_2Sb_2$[39]. The frustrated magnetic moments of spin-glass behaviour may be ascribed to the competition between ferromagnetic and antiferromagnetic interactions among magnetic Mn atoms[40].

Electrical transport measurement is another important characterization method of magnetic semiconductors. In Fig. 4, we perform temperature-dependent resistivity ρ for $(Ba_{1-x}Na_x)F(Zn_{1-y}Mn_y)Sb$ (x = 0.00, y = 0.00; x = 0.05, y = 0.00; x = 0.05, y = 0.05; x = 0.075, y = 0.075; x = 0.10, y = 0.10; x = 0.125, y = 0.125; x = 0.15, y = 0.15; x = 0.175, y = 0.175). Both of the parent compound BaFZnSb and $(Ba_{0.95}Na_{0.05})FZnSb$ where only carriers are introduced show metallic behaviour. The semiconducting behaviour is displayed for all samples with substitutions of (Ba,Na) and (Zn,Mn) simultaneously. Remarkably, the resistivity increases monotonically with the doping level x increasing (except for x = 0.175), similar to that in (La,Ca)(Zn,Mn)SbO[41]. The main cause for that is that carriers are scattered by magnetic fluctuations caused by doped Mn atoms. Similar phenomenon has also been reported in (Ga,Mn)As[42].

4. Summary

To summarize, we successfully synthesized a new 1111-type fluoride-antimonide magnetic semiconductor $(Ba_{1-x}Na_x)F(Zn_{1-x}Mn_x)Sb$ (x = 0.05, 0.075, 0.10, 0.125, 0.15 and 0.175) via Na substitutions for Ba supplying carriers and Mn substitutions for Zn introducing local magnetic moments, respectively. For x = 0.175, the Weiss temperature is up to ~ 16 K. The iso-thermal magnetization measurements at 2 K for $(Ba_{1-x}Na_x)F(Zn_{1-x}Mn_x)Sb$ show clear hysteresis loops, and the coercive field H_C is as large as 12 000 Oe, similar to that in (La,Ba)(Zn,Mn)AsO[17] and (Ba,K)F(Zn,Mn)As[34]. Furthermore, the AC susceptibility measurements show that the system evolves into spin-glass state below T_f. The temperature-dependent resistivity measurements demonstrate that all specimens with Na and Mn codoped display semiconducting behaviour. The Zn-based magnetic semiconductor $(Ba_{1-x}Na_x)F(Zn_{1-x}Mn_x)Sb$, Fe-based surperconductor LaFeAsO and antiferromagnet LaMnAsO have the same ZrSiCuAs-type tetragonal structure, which is possible to make multifunctional heterojunctions. The magnetic semiconductors in fluoride compounds have shown some difference from oxide compounds, and provide new ideas for the development of new materials.

Acknowledgements

The work was supported by the Key R&D Program of Zhejiang Province, China (2021C01002) and NSF of China (No. 12074333).

References

[1] Ohno H. Making nonmagnetic semiconductors ferromagnetic. Science, 1998, 281, 951
[2] Dietl T, Ohno H. Dilute ferromagnetic semiconductors: Physics and spintronic structures. Rev Mod Phys, 2014, 86, 187
[3] Dietl T. A ten-year perspective on dilute magnetic semiconductors and oxides. Nat Mater, 2010, 9, 965
[4] Dietl T, Bonanni A, Ohno H. Families of magnetic semiconductors — an overview. J Semiconduct, 2019, 40, 080301
[5] Gu Y L, Guo S L, Ning F L. Progress on microscopic properties of diluted magnetic semiconductors by NMR and μSR. J Semicond, 2019, 40, 081506
[6] Zhao G Q, Deng Z, Jin C Q. Advances in new generation diluted magnetic semiconductors with independent spin and charge doping. J Semicond, 2019, 40, 081505
[7] Munekata H, Ohno H, von Molnar S, et al. Diluted magnetic III-V semiconductors. Phys Rev Lett, 1989, 63, 1849
[8] Wang M, Campion R P, Rushforth A W, et al. Achieving high curie temperature in (Ga, Mn)As. Appl Phys Lett, 2008, 93, 132103
[9] Chen L, Yang X, Yang F H, et al. Enhancing the Curie temperature of ferromagnetic semiconductor (Ga, Mn)As to 200 K via nanostructure engineering. Nano Lett, 2011, 11, 2584
[10] Ferrand D, Cibert J, Bourgognon C, et al. Carrier-induced ferromagnetic interactions in p-doped $Zn_{1-x}Mn_xTe$ epilayers. J Cryst Growth, 2000, 214/215, 387
[11] Haury A, Wasiela A, Arnoult A, et al. Observation of a ferromagnetic transition induced by two-dimensional hole gas in modulation-doped CdMnTe quantum wells. Phys Rev Lett, 1997, 79, 511
[12] Dietl T, Ohno H, Matsukura F, et al. Zener model description of ferromagnetism in zinc-blende magnetic semiconductors. Science, 2000, 287, 1019
[13] Dietl T, Ohno H, Matsukura F. Hole-mediated ferromagnetism in tetrahedrally coordinated semiconductors. Phys Rev B, 2001, 63, 195205
[14] Reed M L, El-Masry N A, Stadelmaier H H, et al. Room temperature ferromagnetic properties of (Ga, Mn)N. Appl Phys Lett, 2001, 79, 3473
[15] Guo S L, Ning F L. Progress of novel diluted ferromagnetic semiconductors with decoupled spin and charge doping: Counterparts of Fe-based superconductors. Chin Phys B, 2018, 27, 097502
[16] Deng Z, Jin C Q, Liu Q Q, et al. Li(Zn,Mn)As as a new generation ferromagnet based on a 1-2-5 semiconductor. Nat Commun, 2011, 2, 1
[17] Ding C, Man H Y, Qin C, et al. $(La_{1-x}Bax)(Zn_{1-x}Mnx)AsO$: A two dimensional "1111" diluted magnetic semiconductor in bulk form. Phys Rev B, 2013, 88, 041102
[18] Masek J, Kudrnovský J, M8ca F, et al. Dilute moment n-type ferromagnetic semiconductor Li(Zn, Mn)As. Phys Rev Lett, 2007, 98, 067202
[19] Wang X C, Liu Q Q, Lv Y X, et al. The superconductivity at 18 K in Li-FeAs system. Solid State Commun, 2008, 148, 538
[20] Zhao K, Deng Z, Wang X C, et al. New diluted ferromagnetic semiconductor with Curie temperature up to 180 K and isostructural to the n122o iron-based superconductors. Nat Commun, 2013, 4,

1442
[21] Zhao K, Chen B J, Zhao G Q, et al. Ferromagnetism at 230 K in $(Ba_{0.7}K_{0.3})(Zn_{0.85}Mn_{0.15})_2As_2$ diluted magnetic semiconductor. Chin Sci Bull, 2014, 59, 2524
[22] Dunsiger S R, Carlo J P, Goko T, et al. Spatially homogeneous ferromagnetism of (Ga, Mn)As. Nat Mater, 2010, 9, 299
[23] Yang X J, Li Y K, Shen C Y, et al. Sr and Mn co-doped LaCuSO: A wide band gap oxide diluted magnetic semiconductor with T_C around 200 K. Appl Phys Lett, 2013, 103, 022410
[24] Agulyansky A. Main principals of the chemistry of tantalum and niobium fluoride compounds. Elsevier, 2004
[25] Toby B H, Von Dreele R B. GSAS-II: The genesis of a modern open-source all purpose crystallography software package. J Appl Crystallogr, 2013, 46, 544
[26] Johnson V, Jeitschko W. ZrCuSiAs: A "filled" PbFCl type. J Solid State Chem, 1974, 11, 161
[27] Kamihara Y, Watanabe T, Hirano M, et al. Iron-based layered superconductor $La[O_{1-x}F_x]$ FeAs (x = 0.05–0.12) with T_c = 26 K. J Am Chem Soc, 2008, 130, 3296
[28] Kabbour H, Cario L, Boucher F. Rational design of new inorganic compounds with the ZrSiCuAs structure type using 2D building blocks. J Mater Chem, 2005, 15, 3525
[29] Fu L C, Gu Y L, Guo S L, et al. Ferromagnetism in fluoride-antimonide $SrF(Zn_{1-2x}Mn_xCu_x)Sb$ with a quasi two dimensional structure. J Magn Magn Mater, 2019, 483, 95
[30] Dho J, Kim W S, Hur N H. Reentrant spin glass behavior in Cr-doped perovskite manganite. Phys Rev Lett, 2002, 89, 027202
[31] Zhang H J, Zhang R F, Fu L C, et al. $(La_{1-x}Sr_x)(Zn_{1-x}Mn_x)SbO$: A novel 1111-type diluted magnetic semiconductor. Acta Physica Sinica, 2021, 70, 107501
[32] Gu Y L, Zhang H J, Zhang R F, et al. A novel diluted magnetic semiconductor (Ca, Na)(Zn, $Mn)_2Sb_2$ with decoupled charge and spin doping. Chin Phys B, 2020, 29, 057507
[33] Fu L C, Gu Y L, Zhi G X, et al. Drastic improvement of Curie temperature by chemical pressure in N-type diluted magnetic semiconductor Ba(Zn, $Co)_2As_2$. Sci Rep, 2021, 11, 7652
[34] Chen B J, Deng Z, Li W M, et al. New fluoride-arsenide diluted magnetic semiconductor (Ba, K)F(Zn, Mn)As with independent spin and charge doping. Sci Rep, 2016, 6, 36578
[35] Zhi G X, Guo S L, Zhang R F, et al. Cu_2(Zn, Mn)(Sn, Al)Se_4: A diluted magnetic semiconductor with decoupled charge and spin doping. J Magn Magn Mater, 2021, 536, 168064
[36] Liu X F, Matsuishi S, Fujitsu S, et al. Spin-glass-like behavior of $CaNi_{1-x}Mn_xGe$. Phys Rev B, 2011, 84, 214439
[37] Lekshmi P N, Raji G R, Vasundhara M. Re-entrant spin glass behaviour and magneto-dielectric effect in insulating Sm_2NiMnO_6 double perovskite. J Mater Chem C, 2013, 1, 6565
[38] Man H Y, Guo S L, Sui Y, et al. $Ba(Zn_{1-2x}Mn_xCu_x)_2As_2$: A bulk form diluted ferromagnetic semiconductor with Mn and Cu codoping at Zn sites. Sci Rep, 2015, 5, 15507
[39] Yu S, Zhao G Q, Peng Y, et al. (Ba, K)(Zn, $Mn)_2Sb_2$: A new type of diluted magnetic semiconductor. Crystals, 2020, 10, 690
[40] Binder K, Young A P. Spin glasses: Experimental facts, theoretical concepts, and open questions. Rev Mod Phys, 1986, 58, 801
[41] Han W, Zhao K, Wang X C, et al. Diluted ferromagnetic semiconductor (LaCa)(ZnMn)SbO isostructural to "1111" type iron pnictide superconductors. Sci China Phys Mech Astron, 2013, 56, 2026
[42] Jungwirth T, Sinova J, Mašek J, et al. Theory of ferromagnetic (III, Mn)V semiconductors. Rev Mod Phys, 2006, 78, 809

Xueqin Zhao is a PhD candidate in the Department of Physics in Zhejiang University, and works on the synthesis and characterization of novel bulk diluted magnetic semiconductors.

Fanlong Ning works on the synthesis and microscopic characterization of unconventional superconductors and novel magnetic semiconductors.